



Estimation of PV output power in moving and rocking hybrid energy marine ships [☆]



Hongda Liu ^{*}, Qing Zhang, Xiaoxia Qi, Yang Han, Fang Lu ^{*}

College of Automation, Harbin Engineering University, Harbin 150001, China

HIGHLIGHTS

- A mathematical model for characterizing the ship PV output power is developed.
- The impacts of the sea condition and ship type on the PV output power are analyzed.
- The hybrid energy storage system is used to stabilize the PV fluctuation powers.
- A SC configuration method based on maximum half period is applied.

ARTICLE INFO

Article history:

Received 23 January 2017

Received in revised form 13 July 2017

Accepted 14 July 2017

Available online 22 July 2017

Keywords:

Green ship

Photovoltaic power generation on moving body

Photovoltaic power fluctuations

Power estimation

Ship rocking

ABSTRACT

In recent years, the application of solar energy and energy storage to ship power systems has shown promise as a method for both reducing annual carbon and nitrogen oxide emissions and improving ship energy efficiency in the maritime shipping industry. When a ship navigates at sea, it encounters a constant rocking motion that is affected by both the surrounding sea conditions and the ship's navigation parameters. This motion increases the uncertainty involved in using solar energy and accelerates the aging of the ship's energy storage battery to some extent. In this study, a universal mathematical model is established for the power generation by photovoltaic (PV) modules in which both the sea conditions and the ship's integrated motion, including its basic movement along with the motion caused by rocking, are taken into account. Based on this model, the fluctuation characteristics of a ship's PV output power are studied and determined using three different simulation scenarios. A binary energy storage scheme based on a decoupled PV output power is proposed in order to both stabilize the small-period PV power fluctuations and slow the aging of the actual battery caused by rocking. In addition, a super-capacitor (SC) configuration is constructed based on a maximum half cycle. Finally, the optimal energy storage capacities for this green ship are compared under both rocking and moving motion. In the case of rocking motion, the SCs are able to achieve an approximately 24.8–35.0% reduction in battery replacement. A shipping route between Shanghai, China and Sydney, Australia is considered to validate the practicality of implementing the proposed method.

© 2017 Elsevier Ltd. All rights reserved.

1. Introduction

Low-carbon and renewable energy (RE) technologies have attracted considerable attention in recent years [1,2]. Ocean shipping comprises the largest volume of world trade because of its

advantages over other methods of transport in terms of both transportation cost and capacity. According to statistics from the International Maritime Organization [3], the total amount of carbon dioxide generated by international ocean ships is 8.4 billion tons per year, and the sulphur oxide (SO_x) generated by these ships accounts for 4% of total global SO_x emissions. For these reasons, the Maritime Agreement Regarding Oil Pollution sets up several “emission control areas”, and requires ocean ships sailing through these areas to strictly control their emissions of both NO_x and SO_x [4]. Consequently, the integration of renewable energy into green ship power systems has become an important topic of research [5,6]. The use of RE has many advantages over other sources of energy, as explained in [7]. RE can contribute to both maintaining

[☆] This work was supported by Nature Science Foundation of China, Engineering and Physical Sciences Research Council, and National Environment Research Council (5171101175); Nature Science Foundation of China (51109050); Fund Project for Harbin Science and Technology Innovation (2016RQQXJ101); Fundamental Research Funds for the Central Universities (Nos: HEUCFP201710, HEUCFP201714, HEUCFP201715, HEUCF160406).

^{*} Corresponding authors.

E-mail addresses: liuhd405@hrbeu.edu.cn (H. Liu), lufang@hrbeu.edu.cn (F. Lu).

Nomenclature

RE renewable energy
 PV photovoltaic
 PVOP PV output power
 ESS energy storage system

SIM ship-integrated motion
 DOF degree of freedom
 PVPGE PV power generation equipment
 SC super-capacitor

the sustainability of a ship's power supply and protecting the environment [8]. For example, [9] mentioned that the EU initiated a research project to adopt photovoltaic (PV) generation for more than 75 ships, and several projects to promote the application of PV units to ship power systems have also been carried out in Asia [10,11].

In comparison to those installed on land, the PV panels installed on ships have special characteristics. As a green energy ship can be regarded as a moving body, the ship's relative position is time-varying. In addition, the radiation on PV panels under such circumstance is influenced not by the sunlight's angle of incidence but by the ship's latitude and longitude [12]. In light of the above, many researchers are currently engaged in working on hybrid energy systems [12–15]. The authors of [12] compared the multi-faceted differences between PV panels on land and those on ships. In addition, they used the HOMMER software to compare the results of various capacity configurations. Lan et al. [13] was performed on an oil tanker operating between Dalian, China and Aden, Yemen, and aimed to minimize both the investment cost and the CO₂ emissions of the tanker. Meanwhile, the capacities of both the ship's PV panels and its energy storage were optimized using a hybrid MOPSO and NSGA-II optimization algorithm. Lan et al. [14] analyzed the optimal placement angles of PV panels on ships with respect to the latitude and longitude that occur while sailing, and their results suggested that horizontal angles is better.

However, none of the previously mentioned studies considered the angle changes that occur when a ship rocks in the ocean. In real situations, a ship's attitude changes with both its motion and the rocking that it encounters caused by ocean winds and waves. Therefore, the irradiance on its PV panels is time-varying. Only a few researches studies to date have taken the special nature of the PV power generation equipment (PVPGE) on ships into consideration. Wen et al. [15] investigated the PV output power (PVOP) of

ships with respect to both their basic motion and their rocking. Via contrastive experiments, the researchers discovered that the PVOP characteristics change little whether rocking is considered or not. Nevertheless, [15] found that the fluctuating PV power caused by rocking accelerated the aging of the battery to some extent. Several papers show that frequent battery replacement and discharge generally reduce the actual battery capacity available [16,17]. However, small-period on-board PV unit power fluctuations alternately initiate battery charging and discharging. In addition, when the capacity of a battery has decayed to 75% of its original amount, the usage mode that includes shallow charging and discharging has a large effect on the actual surplus capacity of the battery [17]. Moreover, the negligence has an adverse impact on the results of optimization in real situations. Therefore, if the frequency of the power fluctuations is sufficiently high, they may be difficult to stabilize using only the battery.

To mitigate the adverse effects of frequent charging and discharging on the lithium battery's aging, an energy storage device with a large number of charge-discharge cycles (i.e., an SC or a flywheel with low inertia [18,19]) can be introduced to the energy storage system (ESS). Using an improved energy storage system, consisting of the battery and either an SC or a flywheel, is a logical method of improving both the reliability and the stability of the energy supply. Compared to batteries, flywheels usually have higher initial costs and are relatively more difficult to operate. Moreover, their electrically driven devices require large installation spaces. Consequently, flywheels are used primarily in military vessels with electric propulsion [20]. In this paper, a battery and SC design is applied to a hybrid energy system. The structure of a typical on-board hybrid energy system is shown in Fig. 1.

The main contributions of this paper are summarized as follows: (1) a mathematical description of the on-board PVOP that considers both the ship's integrated motion (SIM) and the sea

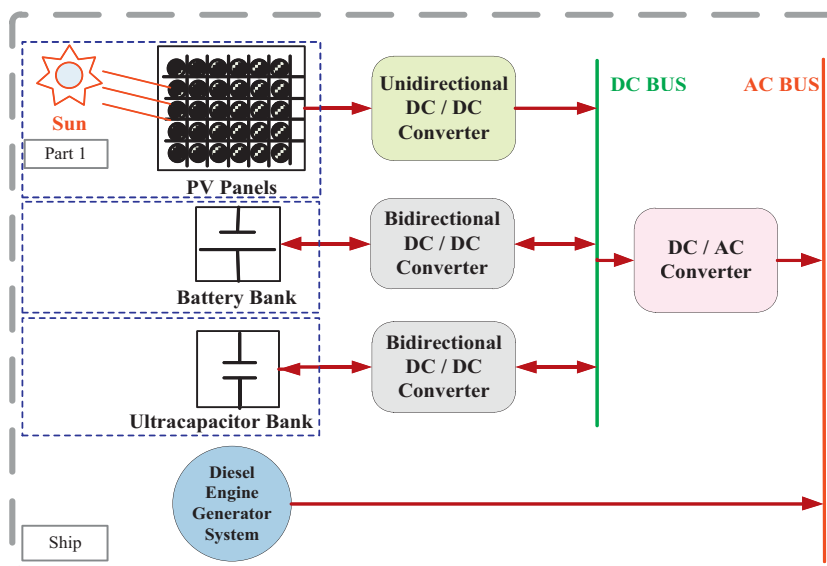


Fig. 1. The structure of a ship hybrid energy system.

conditions is proposed. (2) The proposed solution utilizing an SC along with the battery is shown to stabilize the corresponding section of the decoupled PVOP. (3) To determine both the capacity of the SC and other relevant parameters, an optimal maximum semi-periodic wave energy method is developed. (4) The proposed method can be applied universally to other ships on other routes.

The rest of this paper is organized as follows. In Section 2, a model of the ship's movement is introduced. In Section 3, the extraterrestrial solar irradiance is modeled. In Section 4, both the total solar irradiance on the PV panels and the output power of the PV units are modeled. In Section 5, the practicality of implementing the proposed model is demonstrated. In Section 6, an optimized on-board ESS is studied to investigate the effects of the rocking motion on the battery, and a method for determining the capacity of the SC is presented. Finally, a summary of the study and our conclusions are provided in Section 7.

2. Model of ship motion

While operating at sea, ships sway because of waves, winds and currents. When ships are considered rigid bodies, their movement generally has six degrees of freedom (DOF): rolling, pitching, surging, swaying, heaving and yawing, as shown in Fig. 2. $G - X_b Y_b Z_b$ is the moving coordinate system with respect to the ship, and the ship's center of gravity is the origin. $O - XYZ$ is the coordinate system moving along with the ship, with OXY located on the still water surface and the direction OX representing that of the ship's velocity v . When the ship encounters waves, the coordinate system does not sway along with the ship and still moves forward at its average speed in the original direction. For simplicity, G and O are assumed coincident. The $O_1 - \xi\eta\zeta$ coordinate system uses the Earth as a reference and is used to describe the wave, but it is not depicted in the figures. Whenever the ship sways, the X -axes of the two coordinate systems are coincident and the X_b -axis is used as the rotation axis. The angle between the flat surfaces of the moving coordinate system $GY_b Z_b$ and $GY_x Z_x$ is called the rotation angle φ . Similarly, pitching and yawing rotate around Y_b and Z_b , respectively, and their corresponding roll angles are the pitching angle θ and the yaw angle ψ .

Because of their limited motion damping, ships roll extensively in wind and waves. The effect of rolling on the PVOP is mainly studied in the paper. However, the other five types of ship motion have little impact on rolling. As a result, their effects on the PVOP can be neglected [13], and rolling motion is the focus of this paper.

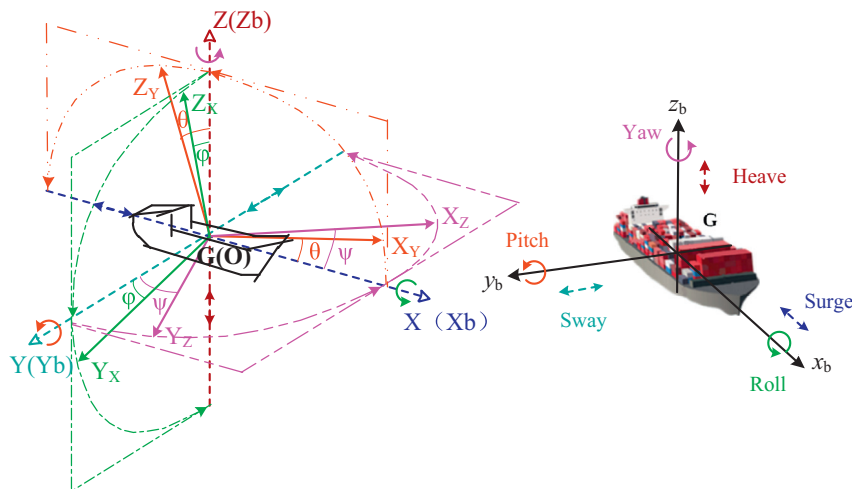


Fig. 2. Mathematical model for 6-DOF motions.

Because of its complexity, models of ship motion involve a large number of random factors. Therefore, it is assumed that the six types of ship motion are mutually independent. When analyzing rolling motion, the relationships between the roll and other degrees of freedom is ignored [21]. In addition, the ship's performance with respect to waves includes the wind as well. Waves are typically described using two-dimensional energy spectra [22]. A model is established for rolling by defining the moment of wave excitation as the sum of the moments of inertia, damping and restoration. When the roll angle is small, the rolling motion of the ship can be described using a linear model (i.e., Connolly's equation) [23]. However, for large roll angles, a linear rolling model cannot reflect the rolling characteristics of the ship accurately. Therefore, a nonlinear model is used to describe the rolling motion. In this paper, we use the nonlinear model shown in the following equation [24,25]:

$$(J_{\varphi\varphi} + \Delta J_{\varphi\varphi})\ddot{\varphi} + M_D(\dot{\varphi}) + K_R(\varphi) = Q_C h \chi_{\varphi} a_0 \sin \omega_e t \quad (1)$$

where φ , $\dot{\varphi}$, and $\ddot{\varphi}$ represent the roll displacement, angular velocity, and angular acceleration, respectively. $J_{\varphi\varphi}$ and $\Delta J_{\varphi\varphi}$ represent the roll moment of inertia and the added moment of inertia, respectively, Q_C is the displacement of the ship, h is the metacentric height, α_0 ($^\circ$) is the wave slope angle, ω_e (rad/s) is the frequency of encountering waves, and t is the time. In addition, $M_D(\dot{\varphi})$ and $K_R(\varphi)$ represent the nonlinear damping and restoration moments, respectively, which are the primary factors in the nonlinear rolling motion of the ship. Finally, χ_{φ} is the compensation factor of the wave slope angle, given by

$$M_D(\dot{\varphi}) = A\dot{\varphi} + B|\dot{\varphi}|\dot{\varphi} \quad (2)$$

$$K_R(\varphi) = K_1\varphi + K_2\varphi^3 \quad (3)$$

$$\chi_{\varphi} = \chi_{\varphi T} \cdot \chi_{\varphi B} \quad (4)$$

where A and B are the damping coefficients obtained via ship model experiments, K_1 and K_2 are coefficients determined by the static characteristics of the vessel, $\chi_{\varphi T}$ is the dynamic pressure correction coefficient, caused by the draft finiteness, that depends on both the ratio between the draft and the wavelength (T/λ) and the cross section of the ship, and $\chi_{\varphi B}$ is the correction coefficient originating from the ship beam finiteness that depends on both the ratio between the ship beam and the wavelength (B/λ) and the cross section of the ship.

In this paper, a linearization method is used to solve Eq. (1). This method consists of two parts: the nonlinear damping moment ($M_D(\dot{\varphi})$) linearization and the nonlinear restoring moment ($M_R(\varphi)$) linearization. The damping moment linearization is solved using the energy equivalence method. It is assumed that $M'_D(\dot{\varphi}) = 2N_e\dot{\varphi}$ is the equivalent linear damping moment of $M_D(\dot{\varphi})$. To ensure the same energy dissipation over equal periods, this moment should comply with

$$\int 2N_e\dot{\varphi}d\varphi = \int (A\dot{\varphi} + B|\dot{\varphi}|\dot{\varphi})d\varphi \quad (5)$$

Moreover, it is assumed that the particular solution of Eq. (1) is

$$\varphi = \varphi_a \sin(\omega t - \varepsilon_{\varphi-a}) = \varphi_a \sin \psi \quad (6)$$

where φ_a is the roll response amplitude and $\varepsilon_{\varphi-a}$ is the phase difference between the roll angle φ and the wave angle a . When the course and speed of the ship are considered, then $\omega = \omega_e = \frac{2\pi}{\lambda}(c + v \cos \chi)$, where c is the wave's velocity and v is the ship's velocity.

Substituting Eq. (6) into Eq. (5), we obtain

$$2N_e = 2N_{\varphi\varphi} + \frac{8}{3\pi} \varphi_a \omega B \quad (7)$$

where $2N_{\varphi\varphi} = N_{\varphi\varphi}(0)(1 + 3.3F_r)$, $F_r = v/\lambda\sqrt{gL_c}$ is the Froude number, g is acceleration due to gravity on Earth, L_c is the length of ship, and $N_{\varphi\varphi}(0)$ is the rolling damping coefficient when the ship has no forward velocity, which can be via by ship model experiments.

By writing a Fourier expansion for the nonlinear term and omitting portions of the higher order terms, we are able to restore the nonlinear restoration moment:

$$\begin{aligned} K_R(\varphi) &= K_1\varphi + K_2\varphi^3 \approx K_1\varphi_a \sin(\omega t + \varepsilon_{\varphi-a}) + \frac{3}{4}K_2\varphi_a^3 \sin(\omega t + \varepsilon_{\varphi-a}) \\ &= (K_1 + \frac{3}{4}K_2\varphi_a^2)\varphi_a \sin(\omega t + \varepsilon_{\varphi-a}) \end{aligned} \quad (8)$$

where $\bar{K} = K_1 + \frac{3}{4}K_2\varphi_a^2$ is the coefficient of the linear roll restoration moment.

After linearizing Eq. (1), we obtain

$$\ddot{\varphi} + 2\nu_e\dot{\varphi} + n_e^2\varphi = n_e^2\chi_\varphi a_0 \sin \omega_e t \quad (9)$$

Where $2\nu_e = \frac{2N_e}{J_{\varphi\varphi} + \Delta J_{\varphi\varphi}}$ is a dimensionless roll damping coefficient,

$n_e = \frac{\bar{K}\varphi_a \sin(\omega t + \varepsilon_{\varphi-a})}{J_{\varphi\varphi} + \Delta J_{\varphi\varphi}}$ is the natural frequency of the motion roll, and

$n_\varphi = \sqrt{\frac{Q_c h}{J_{\varphi\varphi} + \Delta J_{\varphi\varphi}}}$ is the natural frequency of the linear roll. $J_{\varphi\varphi}$ and $\Delta J_{\varphi\varphi}$ can be obtained via ship model experiments.

In Eq. (9), neither the damping moment coefficient nor the moment of restoration is constant, but they can be expressed with a polynomial that is related to the roll angle. Therefore, Eq. (6) is substituted into Eq. (9), and then an iterative method is used to solve it. The analytical solution of Eq. (9) is

$$\varphi_x = \frac{n_e^2 \alpha_{e0}}{\sqrt{(n_e^2 - \omega^2)^2 + (2\nu_e)^2 \omega_e^2}} \quad (10)$$

$$\varepsilon_{\varphi-a} = \arctan \frac{2\nu_e \omega_e}{n_e^2 - \omega_e^2} \quad (11)$$

where $\alpha_{e0} = \chi_\varphi a_0$ is the effective amplitude of the wave slope angle and χ is the course angle caused by both the ship and the wave.

Given all of this, it is clear that ship rolling is related not only to the parameters $J_{\varphi\varphi} + \Delta J_{\varphi\varphi}$, $N_{\varphi\varphi}(0)$ and K_1 , but also to parameters that reflect environmental factors, such as c , v , χ , F_r , and χ_φ . By solving the rolling equation, it is possible to obtain the roll angles under various sets of environmental conditions.

3. Model of extraterrestrial solar irradiance on board

With further analyses and modifications, the model of extraterrestrial solar irradiance on a motion ship can be introduced based on the static model of PV panels.

3.1. PVPGE in a stationary situation

There is a static surface that is perpendicular to the solar beam on a given date. Then the irradiance obtained from the sun on this surface is named as E_n (W/m^2). It can be expressed [26]:

$$E_n = E_{sc}(R_o/R)^2 \quad (12)$$

$E_R = (R/R_o)^2$ is substituted into Eq. (12) and then $E_n = E_{sc}/E_R$ is obtained. E_{sc} is the solar constant and its value equals $1367 W/m^2$. E_R is the revised coefficient of Sun-Earth distance on a given date. When the solar beam is not perpendicular to the given surface, irradiance calculation needs to be revised. Solar incidence angle on any surface is described in Fig. 3. Fig. 3 shows three angles. If the given surface is a surface of PV panel, the angle between PV panel and horizontal plane of the $O_1 - \xi\eta\zeta$ coordinate system is called the inclined angle or B ($^\circ$). If the line connects the center of the sun with any point of PV panels is called sun-PV line, the angle between sun-PV line and normal PV panels is called incidence angle or i ($^\circ$). The angle between the projection line of normal PV panel on the ground and the south direction is called the azimuth angle of PV panel or γ ($^\circ$). Its value is zero in the direction of south, positive in the direction of west, and negative in the direction of east.

Extraterrestrial solar irradiance at any place and any time is named E (W/m^2) and can be expressed [27]:

$$E = E_n \cos i \quad (13)$$

$$\begin{aligned} \cos i &= \sin \sigma_c \sin D_u \cos B - \sin \sigma_c \cos D_u \sin B \cos \gamma \\ &\quad + \cos \sigma_c \cos D_u \cos B \cos \sigma_l + \cos \sigma_c \sin D_u \sin B \cos \gamma \cos \sigma_l \\ &\quad + \cos \sigma_c \sin B \sin \gamma \sin \sigma_l \end{aligned} \quad (14)$$

It is noteworthy that the value of E is zero when $\cos i \leq 0$. To calculate the extraterrestrial solar irradiance on board, the basic parameters, namely the solar declination angle ω_c [28], the latitude D_u where PV panels are located, the inclined angle of PV panels B , the sun hour angle σ_l ($\sigma_l = f(L_u)$) [29], and the azimuth angle of PV panels γ , should be calculated first. In addition, the solar hour angle σ is an expression of time, expressed in angular measurement, usually degrees, from solar noon.

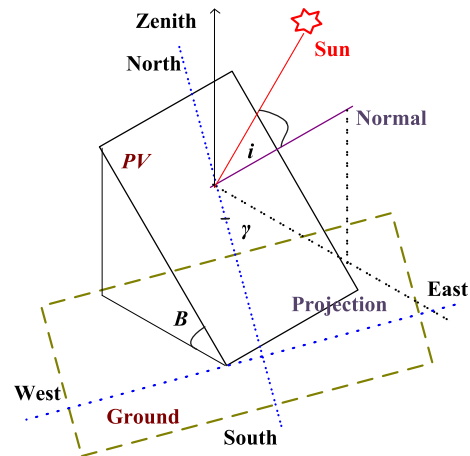


Fig. 3. Schematic diagram of solar incidence angle.

3.2. PVPGE in a moving and rocking situation

If the time horizon is divided into small enough slots, the moving ship can be equivalent to static at each time slot. The model for calculating extraterrestrial solar irradiance of static PV panels described above can be used to obtain the extraterrestrial solar irradiance of the moving PV panels. However, the parameters σ_c , D_u , B , σ and γ should be corrected for a ship with integrated motions.

Assuming that a ship begins its sailing at t_0 hour, M month, D day, Y year, and its cumulative day is N_0 . The coordinate of the departure place is (L_0, D_0) . The longitude L in the eastern hemisphere is positive, and the latitude D in the northern hemisphere is positive. Sailing speed is denoted by V_0 (km/h). The longitude and latitude of the place, where its local time is the standard time of the time zone, is L_{s0} and D_{s0} . Real-time latitude L_u , longitude D_u , azimuth angle γ and the angle between PV panels and horizontal plane B are modified and shown:

$$H_d/H = \begin{cases} 1 - 0.09k_T & (k_T \leq 0.22) \\ 0.9511 - 0.1604k_T + 4.388k_T^2 - 16.638k_T^3 + 12.336k_T^4 & (0.22 \leq k_T \leq 0.80) \\ 0.165 & (k_T > 0.80) \end{cases} \quad (21)$$

$$L_u = L_0 - (180/\pi)(V_0/r)(t/3600) \sin(JD) \quad (15)$$

$$D_u = D_0 - (180/\pi)(V_0/r)(t/3600) \cos(JD) \quad (16)$$

$$\gamma = \begin{cases} JD - 90^\circ & \text{rolling and swing} \\ JD & \text{pitching} \end{cases} \quad (17)$$

$$B = \varphi \pm B_c \quad (18)$$

where JD represents the sailing direction and its value is the angle between the sailing line and the south direction, r is the average radius of the earth and its value is 6371.39 km, B_c is the initial incline angle of PV panels. Lan et al. [14] indicates that installing the PV panels horizontally on deck is the optimal economic way. Therefore, B_c is zero in this paper.

It is assumed that the PV panels lay symmetrically along the ship's axis. When the ship is not rocking and the initial angle of incline of PV panels is zero in the sailing ship, B is zero. If the ship is rocking, the rolling angle is the integration of sinusoidal angular movement of different frequencies [30]. In a small enough period, the variable parameters (i.e., winds, waves, ocean currents and ship's speed) can be regarded as constants, and the superimposed motion can be approximately calculated in Section 2.

Then σ can be revised via the changing latitude, longitude and time, γ can be revised via changing JD , ω_c can be corrected via the sailing time, B can be replaced via φ . Finally, the revised parameters will be substituted in (14) and (13), and E of PVPGE on a motion ship at any time can be determined.

4. Model of total irradiance on PV panels

Internal solar irradiance on a surface (W/m^2) can represent the total solar irradiance on a PV panel. Consequently, the Perez model [31] is used to calculate the irradiance on the PV panels considered in this study. This irradiance comes from three sources [33]: (1) the direct solar irradiance on the panels, (2) the sky-diffuse reflection irradiance, and (3) the ground-reflected irradiance. Thus, the total irradiance can be written as [32]

$$H_T = H_Z + H_S + H_F \quad (19)$$

where H_T is the total solar irradiance on the PV panels, H_Z is the direct solar irradiance, H_S is the sky-diffuse reflection irradiance and H_F is the ground-reflected irradiance.

4.1. Direct solar irradiance

By applying the model of total solar irradiance to the horizontal PV panels, the total direct solar irradiance on the tilted PV panels can be obtained. The total solar irradiance on the horizontal panels, or H , can be expressed [33,34]

$$H = H_b + H_d \quad (20)$$

where H_b represents the total direct solar irradiance on these panels and H_d represents the total irradiance of solar-diffuse reflection that is incident upon them. The percentage of the H_d total solar irradiance on the horizontal PV panels from H_d can be expressed as (21)

where $k_T = H/E$ ($0 \leq k_T \leq 1$) [36] is the clearness index, which has a value close to 1 when few clouds are obscuring the sunlight.

Because of the effects of the diffuse irradiance on the direct irradiance, H_{LZ} is used to represent the modified total direct solar irradiance on the horizontal PV panels, given by

$$H_{LZ} = H_b + H_d A \quad (22)$$

where A is known as an anisotropy factor that is used to determine the nearby solar scattering irradiance and can be calculated using $A = H_b/E$.

Based on the above analysis, the total direct solar irradiance on the tilted PV panels, or H_Z , can be calculated using

$$H_Z = (H_b + H_d A) R_b \quad (23)$$

$$R_b = H_Z/H_{LZ} = \cos i / \sin h \quad (24)$$

$$\sin h = \sin D_u \sin E_c + \cos E_c \cos D_u \cos \omega \quad (25)$$

where h is the solar elevation angle and R_b is the ratio of the solar direct irradiance on the tilted PV panels to the direct solar irradiance on the horizontal PV panels.

4.2. Sky diffuse and ground reflected irradiance

The sky-diffuse and ground-reflected irradiances on the tilted PV panels can be calculated with

$$H_S = H_d(1 - A)[(1 + \cos B)/2][1 + \sqrt{H_b/H} \sin^3(B/2)] \quad (26)$$

$$H_F = \rho_g[(1 - \cos B)/2]H \quad (27)$$

where ρ_g is the surface reflectivity, with values of 0.2 on land and 0.6 at sea.

The total solar irradiance on the tilted PV panels can be acquired by inserting Eqs. (23), (26) and (27) into Eq. (19). The PVOP can be described by [35]

$$P_{pv} = Y_{pv} \cdot f_{pv} \cdot H_T/H_{T,STC} \quad (28)$$

where Y_{pv} (W) is the rated capacity of the PV panels, f_{pv} (%) is their derating factor, and H_T is the total solar irradiance on them.

In addition, $H_{T,STC}$ is the irradiance under standard test conditions, equal to 1000 W/m^2 .

Based on the information presented in Sections 2–4, a mathematical description of the PVOP is obtained. When a ship is sailing, its motion simultaneously includes its forward velocity and swaying based on the collective influence of both its own design factors (e.g., $J_{\varphi\varphi} + \Delta J_{\varphi\varphi}$, Q_C , and h) and the marine environmental factors (e.g. c , ω_e , χ , and v). As the ship's PV panels are fixed on its deck, they follow the movement of the ship. In Section 2, the roll angle φ was obtained to model the ship's motion. In addition, in Section 3, a mathematical model of the ship's moving based on the parameters σ_1 , γ , σ_c , and φ (B) was introduced. Therefore, the extraterrestrial solar irradiance (E) can be obtained for any place and time along the ship's route. In Section 4, a model consisting of H_Z , H_S , and H_F was established that related the rolling parameter B and the motion parameters $\cos i$, σ_c , D_u and D_u influence of the surrounding environment on the PVOP can be accurately described using these mathematical models.

5. Model validation and case analysis

To verify the validity of the proposed model, three scenarios based on a shipping route between Shanghai, China (A) and Sydney, Australia (D), shown in Fig. 4, are considered in calculating the PVOP. In addition, the geographical location, weather, time factor, marine environment, and specific characteristics of the solar hybrid-energy ship are considered along the route. Comparisons are made to demonstrate the influence of the SIM on the PVOP.

The relevant marine environment data are obtained from [37]. The shipping route takes a total of twelve days, and the latitudes and longitudes of places between Shanghai and Sydney are listed in Table 1. The system parameters used in the simulation are shown in Table 2, and the PV data is listed in Table 3.

To facilitate comparisons, three scenarios are considered in calculating the PVOP: Scenario A (swing), in which the PV panels undergo SIM (forward moving and rocking) over the route, Scenario B, in which the PV panels encounter steady (forward moving only), and Scenario C (starting), in which the PV panels are fixed in

Table 1
Latitudes and longitudes between Shanghai and Sydney.

Places	Longitude	Latitude
A. Shanghai	E 121.95°	N 30.90°
B. Yap	E 138.60°	N 5.26°
C. Between New Ireland and Bougainvillea	E 155.11°	S 12.40°
D. Sydney	E 153.14°	S 24.63°

Table 2
Parameters in the simulation.

Parameters	Symbol	Value
Ship parameters	Length	L_c 116 m
	Width	W_c 18 m
	Depth	D_c 8.35 m
	Displacement	Q_c 5878.8t
	Waterline coefficient	C_w 0.5595
	Actual depth of the draft	d 5.4 m
Voyage information of starting point	Year	Y 2015
	Mouth	M 10
	Day	D 2
	Latitude	L_0 E 122°
	Longitude	D_0 N 31°
	Sailing speed	V_0 15 kn
Heading direction	JD_0 -33	
Irradiance on PV panels	Solar constant	E_{sc} 1367 W/m^2
	Earth radius	r 6371.39 km
	Clearness index	K_T 0.8
	Surface reflectance	ρ_g 0.6

Table 3
PV data.

Efficiency	0.17
PV panel area	1.25 m^2
Lifetime	25 year
Replacement cost	\$1500/kW
Installation cost	\$1800/kW



Fig. 4. Shipping Route between Shanghai and Sydney.

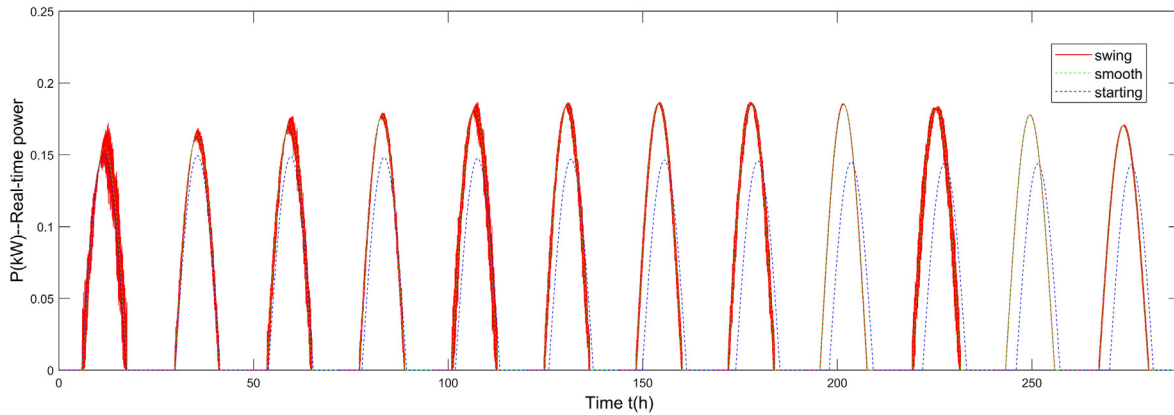


Fig. 5. The PV unit power in three scenarios (swing\smooth\starting).

place as the ship is docked. To simplify the simulation scenarios, the solar ship begins sailing from Shanghai to Sydney at 00'clock on October 2nd, 2015, and this is used as the starting time for the simulation calculations. To verify the validity of the proposed model and reveal the differences between scenarios, it is assumed in this section that 1-kw-capacity PV panels are used on the ships. The output power of the PV units under these three scenarios is simulated, and the results are shown in Fig. 5.

At the beginning of the trip, the direct solar irradiance point is slightly south of the Equator, because the date is October 2nd, 2015. This point continues moving slowly south. When the ship gets closer to the direct solar irradiance point, both the amount of extraterrestrial solar irradiance it encounters on sunny days and the maximum daily output power (P_{max}) increase. Fig. 5 shows that the maximum daily powers output by the PV panels in Scenarios A and B are larger than that of Scenario C. Suppose that no sudden weather changes occur during the voyage. For Scenarios A and B, the maximum power P_{max} continues increasing until the ship arrives at the direct solar irradiance point, where P_{max} achieves its highest value. After that, P_{max} begins decreasing, but it remains larger than that of Scenario C. The changes in the PV unit power for the three scenarios are consistent with what actual occurs.

The PVOP curve over the 1080 s between 11:42 and 12:00 on the first day of the trip is shown in Fig. 6 and illustrates that its value fluctuates along with the rocking motion. If the ship undergoes constant moving without rocking (i.e., Scenario B), the PVOP increases smoothly, without fluctuations. The change in the amplitude of the PVOP indirectly reflects the change in the roll angle

under various operating and marine conditions. The fluctuation of the PVOP with respect to the green line is similar to the rolling motion that rotate around the axis OX_b . The maximum PV power is 0.189 kW under standard irradiance conditions (25 °C and, 1000 W/m²). The PV power in Scenario A is denoted by P_y , and, similarly, the PV power in Scenario B is denoted by P_k . Fig. 6 shows the results Fig. 5 in greater detail. The percentage difference between P_y and P_k on the first day is presented in Fig. 7. As shown in the figure, the power fluctuations that occur between 8:00 and 14:00 are lower than 20%, while the PVOP varies greatly at both sunrise and sunset. These differences are influenced by \cos_i , and the percent difference that originates from P_k . \cos_i is large between 8:00 and 14:00. Although P_k is much larger than $P_y - P_k$, it is not large enough to cause a large percent difference between P_y and P_k . Similarly, \cos_i causes smaller differences at sunrise or sunset, but the difference between P_k and $P_y - P_k$ is also small. Therefore, a large percent difference is obtained. Fig. 6 shows that the power fluctuates frequently, which indicates that the storage device connected to the PV panels may frequently alternate between charging and discharging. If the energy storage consists entirely of batteries, their aging will accelerate due to frequent charging and discharging [16]. Therefore, the power fluctuations obtained in this paper should be considered to avoid the risk of accelerating battery aging.

The total amount of energy generated by the PV units over the (twelve-day) trip under each of the three scenarios is shown in Fig. 8, with the columns representing the energy generated daily. The direct solar irradiance point is slightly south of the equator,

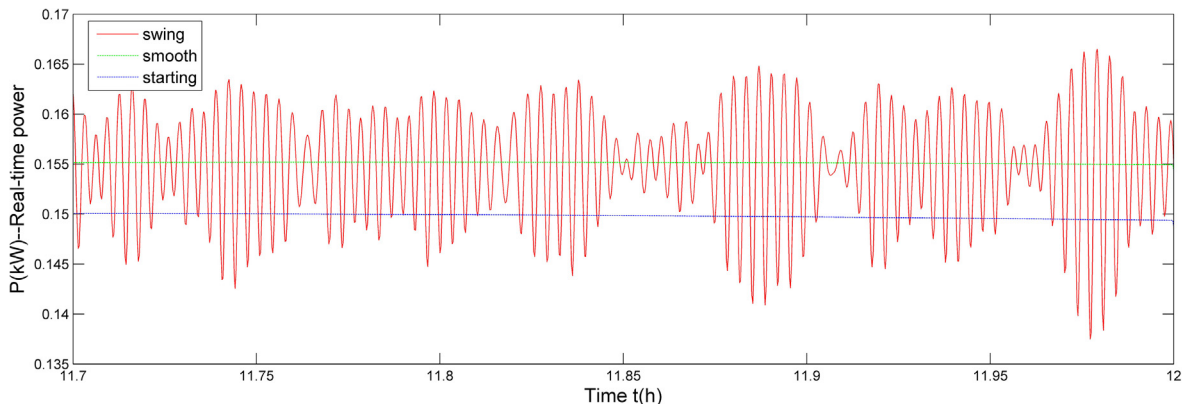


Fig. 6. PVOP curve under the three scenarios (swing\smooth\starting).

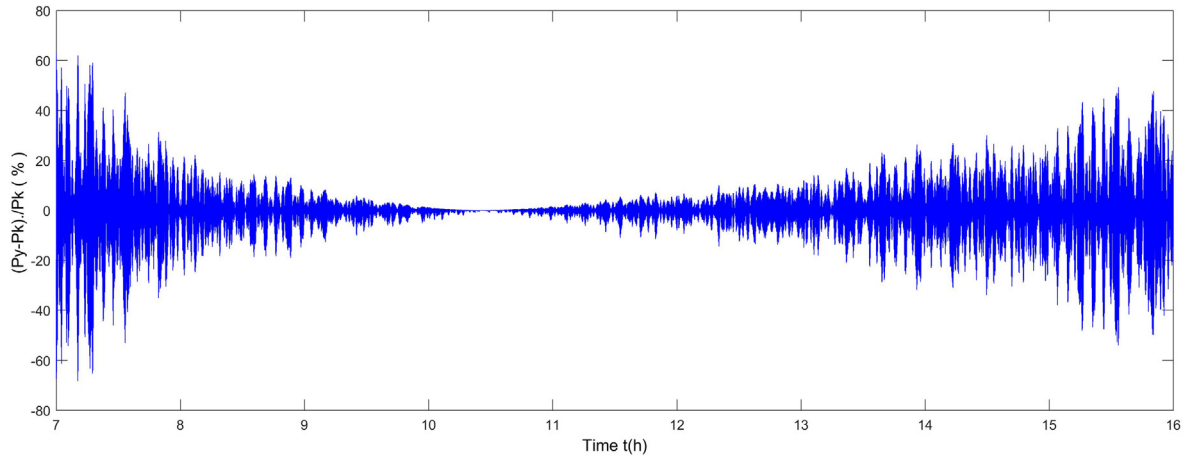


Fig. 7. The percentage of difference between P_y and P_k during the voyage.

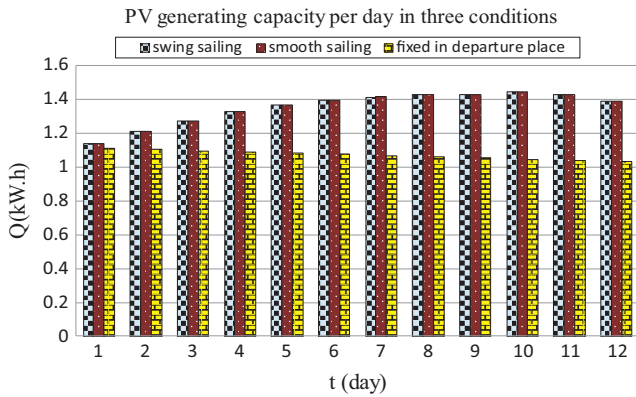


Fig. 8. Generated energy of PV units under three conditions during October 2nd–13rd, 2015.

because the trip begins in October. Therefore, the ship first approaches the perihelion before moving away from it. The energy generated daily and the total power produced over entire trip in Scenario A are represented by Q_y and Q_{yall} , respectively. Similarly, the corresponding variables for Scenario B are Q_k and Q_{kall} , and those for Scenario C are Q_s and Q_{sall} . It is assumed no sudden weather changes take place during the trip. Q_y and Q_k first increase and then gradually decrease, and the value of Q_y is always lower than that of Q_k . In Scenario C, although the ship is always in Shanghai harbor, Q_s decreases with time, as the sun moves slowly southward over the twelve days.

Similarly, based on a large data set of simulation results for diverse marine environments, the ranges of the total generated energy for the other three seasons are obtained and shown in Table 4.

The simulation results provided above indicated that the total difference between Q_{yall} and Q_{kall} is small. Using PV panels with the same capacities, the results calculated for integrated motion are similar to those of moving along with respect to both energy-saving and emission-reduction. Moving has a low computational

complexity. Therefore, the economic benefits of the PV on board can be estimated by calculating the results of such motion. However, frequent power fluctuations occur in Scenario A on the basis of the PV power used in Scenario B. In addition, the amplitudes of the power fluctuations vary. If a battery is applied to stabilize these fluctuations in the PV panels, it may both increase the frequency of the discharge cycles and accelerate the aging of battery to some extent.

6. Capacity selection of energy storage and discussion

6.1. Method of decoupling PV power

The results provided above indicate that the PVOP differs under various scenarios. The differences between the PVOPs in Scenarios A and B are mainly caused by power fluctuations. The power in Scenario A, or P_y , varies more frequently. P_y can be generally regarded as a combination of the power in Scenario B, or P_k , (which is determined by both the intermittency and the randomness of the PV generation) and the power fluctuations (or $P_y - P_k$) associated with ship rocking. A battery was added to absorb P_k , and its capacity of the battery was calculated in [13]. If a ship is not equipped with certain specialized equipment for absorbing $P_y - P_k$, the frequent and shallow battery charge and discharge accelerates its aging to some extent, increases the cost of replacing energy storage devices, and reduces overall efficiencies of both PVPGE and hybrid energy systems [38]. Therefore, it is not reasonable to adopt batteries alone for energy storage in ship power systems with PVPGE. In our study, an SC is used to absorb the power fluctuation caused by rocking.

6.2. Method of calculating SC

Assuming that both moving and rocking coexist while a ship is sailing, the capability of the SC (C_{sc}) is considered for Scenario A

Table 4
Total generated energy of PV units in four seasons during navigation.

	1.2–1.13 (Winter)	3.30–4.10 (Spring)	6.30–7.11 (Summer)	10.2–10.13 (Autumn)
Q_{yall} (kW h)	[15.829, 15.981]	[15.573, 15.58]	[14.116, 14.980]	[16.204, 17.210]
Q_{kall} (kW h)	[15.837, 16.256]	[15.583, 15.849]	[14.129, 15.220]	[16.204, 17.500]
Q_{sall} (kW h)	[10.363, 11.270]	[15.842, 16.132]	[18.677, 19.200]	[12.819, 14.368]
$(Q_{yall} - Q_{kall}) / Q_{kall}$ (%)	[-1.690, -0.036]	[-1.70, -0.07]	[-1.60, -0.102]	[-1.71, -0.033]
$(Q_{yall} - Q_{sall}) / Q_{sall}$ (%)	[41.8, 52.75]	[-7.4, -3.465]	[-26.9, -24.424]	[13, 26.398]

Table 5
SC and battery data.

Parameters	SC	Battery (LiFePO ₄)
Life time	25 years	5 years
Cost of investment	\$7.56/monomer	\$42/kW h
Cost of replacement	-	\$42/kW h

alone. The method of determining C_{sc} used in [38] is applied in this paper. Based on [39], the capability of the SC is determined as follows:

$$P_{sc,rated} \geq \max(|P_{sc}(t)|) \tag{29}$$

$$\Delta E_{sc} = \max \left(\left| \int_{t_1}^{t_2} (P_k - P_y) dt \right|, \left| \int_{t_2}^{t_3} (P_k - P_y) dt \right|, \dots \right) \tag{30}$$

$$V_{ref} = V_{sc,max} / \sqrt{2} \tag{31}$$

$$E_{sc,rated} = \Delta E_{sc} / 0.75 \tag{32}$$

$$C_{sc,min} = 2E_{sc,rated} / V_{sc,max}^2 \tag{33}$$

where $P_{sc,rated}$ is the rated power of the SC, which should be higher than the power it needs at each time step, ΔE_{sc} is the maximum value of all of the total energy, $V_{sc,max}$ is the rated voltage of the SC, and V_{ref} is the reference voltage. Eq. (32) ensures that the SC's utilized energy is only 75% of the total available energy. Finally, $C_{sc,min}$ is the capacity of the SC.

6.3. Optimized energy storage design and discussion

To analyze the impact of the rocking motion on the battery, the optimal ESS for a ship is investigated to minimize both economic costs and carbon emissions. There are three methods of optimizing the ESS when PV panels of the same capacity are used, which are based on the ship's type and its route, as mentioned in Section 5. Method 1 adopts multi-objective particle swarm optimization without considering the swing of the ship. Method 2 adopts the

Table 6
Parameters in four seasons during navigation.

	Sea state levels	Significant wave height (m)	Mean wave period (s)	Wind speed (m/s)	Speed of ship (kn)
Spring	[4,5]	[1.7, 2.6]	[8.3, 10.6]	[7.7, 10.8]	[14,18]
Summer	[3,6]	[0.9, 3.9]	[7.4, 11.0]	[5.4, 12.1]	[15,19]
Autumn	[2,6]	[0.5, 3.6]	[8.1, 11.2]	[3.4, 8.9]	[14,18]
Winter	[4,5]	[1.4, 2.8]	[4.7, 9.3]	[6.5, 11.4]	[12,18]

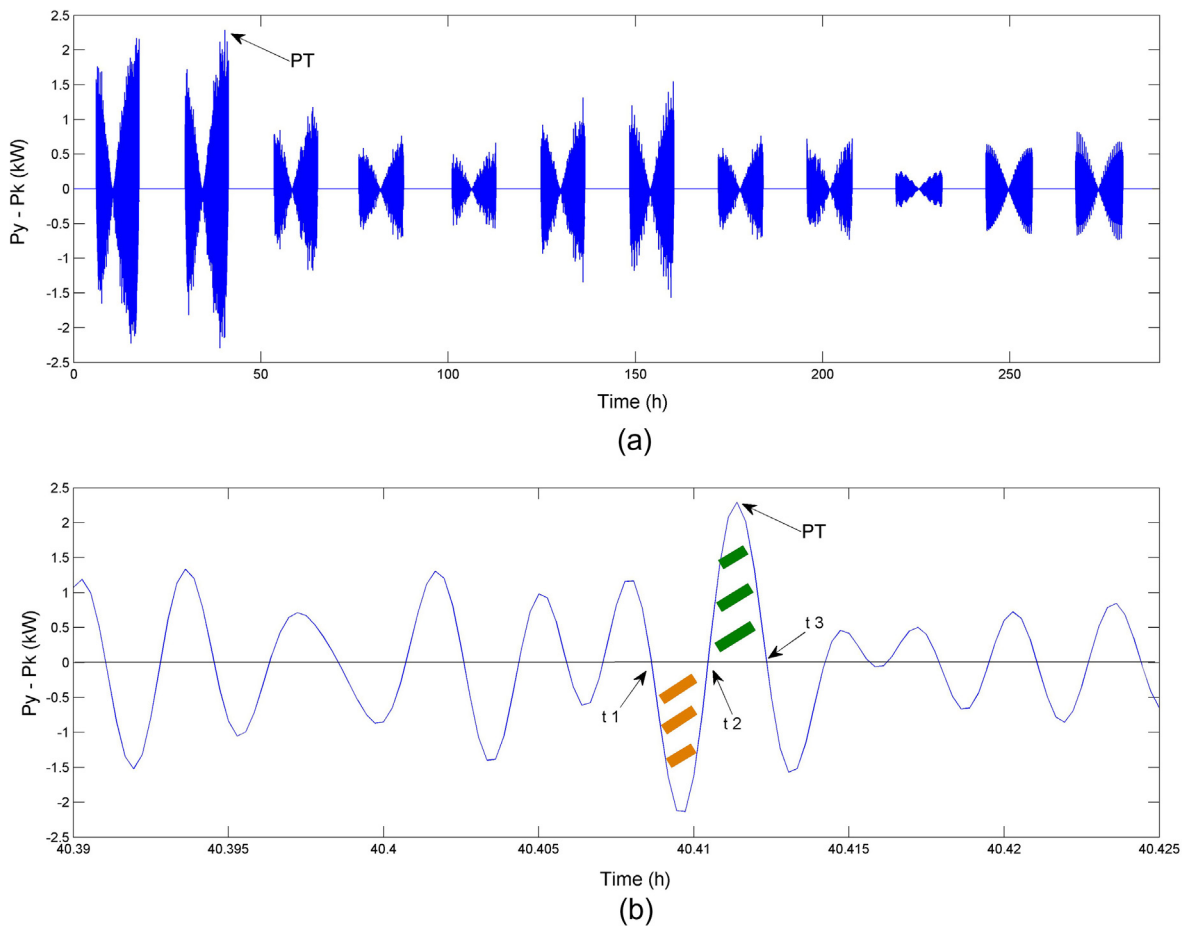


Fig. 9. The curve of difference between P_k and P_y .

interval optimization from [15], which considers the ship's swing. Meanwhile, the roll angle is 16° and the roll period is 20 s. The ESSs of Method 1 and 2 utilize only batteries. In this paper, both a decoupling method and the maximum semi-periodic wave energy are proposed for considering the swinging of a ship (Method 3). The ESS of Method 3 consists of an SC and batteries. The PV power caused by integrated motion is decoupled into two parts: P_k and $P_y - P_k$, which is associated with ship rocking. The SC is used to stabilize the value of $P_y - P_k$ via maximum semi-periodic wave energy, and the batteries are used to stabilize the value of P_k via multi-objective particle swarm optimization. The technical parameters of both the SC and the battery are listed in Table 5. The other relevant equations and parameters regarding the economic cost and the carbon emissions can be found in [13].

Some of the main parameters influencing the PVOP are the sea-state levels, significant wave heights, wind speed, and so on. Changes in these factors result in SC capacity variations. Therefore, the parameters relevant to the “Shanghai-Sydney” route mentioned in Section 5 are segmented statistically, and their representative ranges are obtained in [37]. Table 6 shows the ranges of the influential parameters along the route from A to B. The significant wave heights, generally increases as the wind speed increases. In addition, the route is affected to a greater extent by the wind in both the summer and the winter. For the parameter range of Scenario A, shown in Table 6, the Latin hypercube sampling method [40,41] is used for generating the simulated environment of the ship as it navigates, and the size of the SC is calculated for different scenarios.

The results show that the parameters that require the maximum SC size are a sea-state level of 6, a significant wave height of 3.8 m, and a wind speed between 10.4 m/s and 10.9 m/s in summer. The difference between P_k and P_y with respect to time integration is the energy released or absorbed by the SC, shown in Fig. 9. Fig. 9(a) shows the difference between P_k and P_y over the ship's entire trip, and Fig. 9(b) shows the semi-periodic wave energy of the SC for the maximum moment. In Fig. 9(b), the green portion indicates the released energy and the orange portion indicates the absorbed energy.

The DC bus voltage is 220 V, and the SCs are connected to the DC bus in parallel. Based on the difference between P_k and P_y over the 12-day voyage, ΔE_{sc} is 16754.04 J. The SC used is MAXWELL: BCAP0050 P270 T01, with a monomer-rated voltage of 2.7 V, an absolute maximum current of 27 A, and a rated capacitance of 50 F. A total of eighty SC monomers are connected in series to form a group, and the group is then connected in parallel to form an SC tank. It is estimated that the total mass of the SCs is 1.04 kg, and their total volume is $80 \times 9 \text{ mm}^2 \times 41 \text{ mm}$.

Table 7 presents the annual capital cost of the ESS and the PV cost associated with the optimal ESS capacity for Method 1, 2 and 3.

Table 7 allows the optimal capacities of the three cases to be compared. The ESS cost of Method 1 is \$ 505, which is lower than those of Methods 2 and 3. Because Method 1 does not consider the effects of rolling motion on the PV power, the capacity of the ESS cannot absorb the total PV power. In addition, the rolling motion

can increase the number of battery replacements required during the trip, primarily because rocking increases the frequency of alternation between battery charging and discharging. Comparing Methods 2 and 3, Method 3 achieves a reduction in the ESS battery capacity of between approximately 24.8–35.0%. In addition, the annual ESS capital cost can be reduced by approximately 16.5–27.8%. Over a longer period, the SC can decrease the number of replacement times of the battery, because it has a long life-span compared to the battery. Therefore, the proposed binary energy storage scheme outperforms the ESS (which contains only battery) in improving the economical operation of the ship's power system.

7. Conclusions

In contrast to PV arrays mounted on land, the PVOP on ships is affected by their rocking, which produces power fluctuations with periods of approximately 10–20 s. This causes the actual usable capacity of the battery to degrade from its theoretically predicted value. In addition, the characteristics of PV generation on ships are studied by establishing a mathematical model that considers both the SIM and the actual sailing parameters. Then, based on these characteristics, the paper proposes both a PVOP-decoupling process and an SC-configuration method utilizing the maximum half-cycle fluctuation energy. Finally, the validity of the method is verified by simulating its performance on a shipping route between Shanghai and Sydney.

The major conclusions of this study can be summarized as follows: (1) the rolling motion of a hybrid solar ship negatively affects its battery capacity. Therefore, an optimal ESS design should be considered; (2) rolling causes periodic fluctuations in PV generation, and the characteristics of these fluctuations (including the period and the amplitude) change constantly with respect to both the ship's navigation and the marine conditions; (3) decoupling the PVOP and determining the capacity of its SC based on the maximum half-period is a practical solution to these problems. The results of the study provide new insights for scientific planning, the allocation of economic dispatch and power regulation for green ships with ESSs.

References

- [1] Hidy GM, Chow JC, England GC, Legge AH, Lloyd AC, Watson JG. Energy supplies and future engines for land, sea, and air. *J Air Waste Manage Assoc* 2012;62:1233–48.
- [2] Fernández Soto JL, Garay Sejo R, Fraguera Formoso Ja, Gregorio Iglesias G, Carral Couce L. Alternative sources of energy in shipping. *J Navig* 2010;63:435–48.
- [3] Ovidiu Cristea, Mihai-Octavian Popescu, Aurelian Sorinel Calinciuc. A correlation between simulated and real PV system in naval conditions. In: 2014 International system on fundamentals of electrical engineering. University Politehnica of Bucharest; 2014. p. 1–6.
- [4] Cogliolo Andrea. Sustainable shipping green innovation for the marine industry. Sustainable management of the mediterranean. *Rend Fis Acc Lincei* 2015;26:65–72.
- [5] Ovrum E, Bergh TF. Modelling lithium-ion battery hybrid ship crane operation on stage. *Appl Energy* 2015;152:162–72.
- [6] Alfonsín Víctor, Suarez Andres, Cancela Angeles, Sanchez Angel, Maceiras Rocio. Modelization of hybrid systems with hydrogen and renewable energy oriented to electric propulsion in sailboats. *Int J Hydrogen Energy* 2014;39:11763–73.
- [7] Vinod Kumara RL, Shrivastav SP. Untawalec solar energy: review of potential green & clean energy for coastal and offshore applications. *Science Direct* 2015;4:473–80.
- [8] Lau KY, Yousof MFM, Arshad SNM, Anwari M, Yatim AHM. Performance analysis of hybrid photo-voltaic or diesel energy system under Malaysian conditions. *Energy* 2010;5:3245–55.
- [9] Loois G, Wouters FPH, Koerts GM, van der Weiden TCJ. Monitoring results of PV for electric propulsion in recreational boating. *ECOFYS Consult Res* 1994;1157–60.
- [10] Lee Kyoung-Jun, Shin Dong-Sui, Lee Jong-Pil. Hybrid photovoltaic/diesel green ship operating in standalone and grid-connected mode in South Korea – experimental investigation. *IEEE vehicle power and propulsion conference (VPPC)*; 2012. p. 580–3.

Table 7

Comparison of optimal capacity in three methods.

	Method 1	Method 2 [15]	Method 3
PV size (kW)	51.75	51.75	51.75
ESS capacity (kW h)	24	[31.92, 36.97]	24
SC capacity (F)	–	–	0.462
PV cost (\$)	16001.61	16001.61	16001.61
SC cost (\$)	–	–	56.64
ESS cost (\$)	505	[672.7, 777.92]	561.64

- [11] Lee Kyoung-Jun, Shin Dongsul, Yoo Dong-Wook. Hybrid photovoltaic or diesel green ship operating in standalone and grid-connected mode – experimental investigation. *Energy* 2013;49:475–83.
- [12] Diab Fahd, Lan Hai, Ali Salwa. Novel comparison study between the hybrid renewable energysystems on land and on ship. *Renew Sustain Energy Rev* 2016;63:452–63.
- [13] Lan Hai, Wen Shuli, Hong Ying-Yi, Yu David C, Zhang Lijun. Optimal sizing of hybrid PV/diesel/battery in ship power system. *Appl Energy* 2015;158:26–34.
- [14] Lan Hai, Dai Jinfeng, Wen Shuli, Hong Ying-Yi, Yuand David C, Bai Yifei. Optimal Tilt Angle of Photovoltaic Arrays and Economic Allocation of Energy Storage System on Large Oil Tanker Ship. *Energies* 2015;11:515–30.
- [15] Wen Shuli, Lan Hai, Hong Ying-Yi, Yu David C, Zhang Lijun, Cheng Peng. Allocation of ESS by interval optimization method considering impact of ship swinging on hybrid PV/diesel ship power system. *Appl Energy* 2016;175:158–67.
- [16] Lunz B, Walz Hsauer DU. Optimizing vehicle-to-grid charging strategies using genetic algorithms under the consideration of battery aging. In: *Proceedings of 2011 IEEE vehicle power and propulsion conference*; 2011. p. 1–7.
- [17] Fei Gao, Kai Yang, Dong Hui, Dahe Li. Cycle-life energy analysis of LiFePO₄ batteries for energy storage. *Proc CSEE* 2013;33:41–5 [in Chinese].
- [18] Kollimalla Sathish Kumar, Mishra Mahesh Kumar, Lakshmi Narasamma N. Design and analysis of novel control strategy for battery and supercapacitor storage system. *IEEE Trans Sustain Energy* 2014;5:1137–44.
- [19] Ramlia Makbul AM, Hiendro Ayong, Twaha Ssenoga. Economic analysis of PV/diesel hybrid system with flywheel energy storage. *Renew Energy* 2015;78:398–405.
- [20] Saghaleini Mahdi, Mazloomzadeh Ali. Agent based control scheme for a smart power system including renewable energy sources. In: *2011 International Conference on Environment and Electrical Engineering*; 2011. p. 1–4.
- [21] Loyd ARJM. *Seakeeping: ship behaviour in rough weather*. Ellis Horwood Limited; 1989.
- [22] Malara Giovanni, Spanos Pol D, Arena Felice. Maximum roll angle estimation of a ship in confused sea waves via a quasi-deterministic approach. *Probab Eng Mech* 2014;75–81.
- [23] Moradia Morteza, Malekizade Hamid. Robust adaptive first–second-order sliding mode control to stabilize the uncertain roll dynamic. *IEEE Ocean Eng* 2013;69:18–23.
- [24] Chai W, Naess A, Leira BJ. Stochastic nonlinear ship rolling in random beam seas by the path integration method. *Probab Eng Mech* 2016;44:43–52.
- [25] Zhu HT, Duan LL. Probabilistic solution of non-linear random ship roll motion by path integration. *Int J Non-Linear Mech* 2016;83:1–8.
- [26] Spencer JW. Fourier series representation of the position of the Sun. *Search* 1971;2:172.
- [27] Muneer T, Saluja GS. A brief review of models for computing solar radiation on inclined surfaces. *Energy Convers Manage* 1982;25:443–58.
- [28] Yaoo Yingxue, Hub Yeguang, Gao Shengdong. A multipurpose dual-axis solar tracker with two tracking strategies. *Renew Energy* 2014;72:88–98.
- [29] Kim Y, Han GY, Seo T. An evaluation on thermal performance of CPC solar collector. *Int Commun Heat Mass Transf* 2008;35:446–57.
- [30] van Daalen EFG, Gusing M, Grasman J. Roll dynamics of a ship sailing in large amplitude head waves. *J Eng Math* 2014;89:137–46.
- [31] Perez R, Stewart R, Arbogast C, Seals R, Scott J. An anisotropic hourly diffuse radiation model for sloping surfaces: description, performance, validation, site dependency evaluation. *Sol Energy* 1986;36:481–97.
- [32] Jakhriani AQ, Samo SR, Rigit ARH, et al. Selection of models for calculation of incident solar radiation on tilted surfaces. *World Appl Sci J* 2013;22(9):1334–43.
- [33] Jakhriani Abdul Qayoom, Othman Al-Khalid, Rigit Andrew RH. Estimation of incident solar radiation on tilted surface by different empirical models. *Int J Sci Res Publ* 2012;2(12):1–6.
- [34] National Renewable Energy Laboratory (NREL). Energy modeling software for hybrid renewable energy systems [EB/OL]. [2016-07-19]. <http://usersupport.homerenergy.com/customer/en/portal/articles/2186872-how-homer-calculates-the-radiation-incident-on-the-pv-array>.
- [35] National Renewable Energy Laboratory (NREL). Energy modeling software for hybrid renewable energy systems [EB/OL]. [2016-07-19]. <http://usersupport.homerenergy.com/customer/en/portal/articles/2186875-how-homer-calculates-the-pv-array-power-output>.
- [36] Orgill JF, Hollands KGT. Correlation equation for hourly diffuse radiation on a horizontal surface. *Sol Energy* 1977;19:357–9.
- [37] National Marine Environmental Forecasting Center (China). Available: <http://www.nmefc.gov.cn/hyqh/eerninuo.aspx>.
- [38] Dunlop JP, Farhi BN. Recommendations for maximizing battery life in photovoltaic systems: a review of lessons learned. In: *Proceedings of forum 2001 solar energy: the power to choose*; 2001.
- [39] Wickramasinghe Damith B, Abeywardana Branislav Hredzak, Agelidis Vassilios G. Single-phase grid-connected LiFePO₄ battery–supercapacitor hybrid energy storage system with interleaved boost inverter. *IEEE Trans Power Electron* 2015;30:5591–604.
- [40] Mckay MD, Beckman RJ, Conover WJ. A comparison of three methods for selecting values of input variables in the analysis of output from a computer code. *Technometrics* 1979;21:239–45.
- [41] Yu H, Chung CY, Wong KP, et al. Probabilistic load flow evaluation with hybrid Latin hypercube sampling and cholesky decomposition. *IEEE Trans Power Syst* 2009;24:661–7.